7. D. E. Rummelhart and J. L. McClelland, Eds., *Parallel Distributed Processing: Explorations in the Microstructure of Cognition* (MIT Press, Cambridge, MA, 1986); D. E. Rummelhart, in *Foundations of Cognitive Science*, M. I. Posner, Ed. (MIT Press, Cambridge, MA, 1989), pp. 133–159.
8. R. J. Richards, *Darwin and the Emergence of Evolutionary Theories of Mind and Behavior* (Univ. of Chicago Press, Chicago, 1987).
9. J. E. R. Staddon, *Adaptive Behavior and Learning* (Cambridge Univ. Press, Cambridge, 1983); E. M. Macphail, *Behav. Brain Sci.* **10**, 645 (1987); J. R. Anderson, *ibid.*, p. 467; F. M. Wuketits, *Evolutionary Epistemology* (SUNY Press, Albany, NY, 1990).
10. D. F. Sherry and D. L. Schacter, *Psychol. Rev.* **94**, 439 (1987); B. Wilson, N. J. Mackintosh, R. A. Boakes, *Q. J. Exp. Psychol. B* **37**, 313 (1985); S. J. Shettleworth, in *Advances in Analysis of Behavior*, M. Zeiler and P. Harzem, Eds. (Wiley, New York, 1983), pp. 1–39; J. R. Krebs, S. D. Healy, S. J. Shettleworth, *Anim. Behav.* **39**, 1127 (1990); R. P. Balda and A. C. Kamil, *ibid.* **38**, 486 (1989); P. H. Harvey and J. R. Krebs, *Science* **249**, 140 (1990).
11. L. A. Real, *Ecology* **62**, 20 (1981).
12. D. Bernoulli, *Commentar. Acad. Sci. Imp. Petropaolitanae* **5**, 175 (1738) [for an English translation, see L. Sommer, *Econometrica* **22**, 23 (1954)].
13. J. von Neumann and O. Morganstern, *Theory of Games and Economic Behavior* (Princeton Univ. Press, Princeton, NJ, 1944).
14. S. French, *Decision Theory* (Halstead Press, New York, 1986); R. L. Keeney and H. Raiffa, *Decisions with Multiple Objectives* (Wiley, New York, 1976).
15. H. Markowitz, *Portfolio Selection* (Wiley, New York, 1959); J. Tobin, *Rev. Econ. Stud.* **25**, 65 (1958).
16. L. A. Real, J. R. Ott, E. Siverfine, *Ecology* **63**, 1617 (1982).
17. T. Caraco, S. Martindale, T. Whittam, *Anim. Behav.* **28**, 820 (1980); T. Caraco, *Behav. Ecol. Sociobiol.* **8**, 213 (1981).
18. T. Caraco, *Behav. Ecol. Sociobiol.* **12**, 63 (1983).
19. J. M. Wunderle and T. G. O'Brien, *ibid.* **17**, 371 (1986).
20. C. J. Barnard and C. A. J. Brown, *ibid.* **16**, 161 (1985).
21. F. R. Moore and P. A. Simm, *Experientia* **42**, 1054 (1986).
22. R. C. Battalio, J. H. Kagel, D. N. McDonald, *Am. Econ. Rev.* **75**, 596 (1985).
23. R. J. Herrnstein, *J. Exp. Anal. Behav.* **7**, 179 (1964); M. Davison, *ibid.* **12**, 247 (1969).
24. R. V. Carter and L. M. Dill, *Behav. Ecol. Sociobiol.* **26**, 121 (1990); K. D. Waddington, T. Allen, B. Heinrich, *Anim. Behav.* **29**, 779 (1981).
25. T. Caraco and S. L. Lima, *Quant. Anal. Behav.* **6**, 1 (1986).
26. L. A. Real and T. Caraco, *Annu. Rev. Ecol. Syst.* **17**, 371 (1986); D. W. Stephens and J. R. Krebs, *Foraging Theory* (Princeton Univ. Press, Princeton, NJ, 1986); J. R. Krebs and A. Kacelnik, in *Behavioral Ecology*, J. R. Krebs and N. B. Davies, Eds. (Blackwell, Oxford, 1991).
27. J. M. Henderson and R. E. Quandt, *Microeconomic Theory: A Mathematical Approach* (McGraw-Hill, New York, 1980).
28. L. D. Harder and L. A. Real, *Ecology* **68**, 1104 (1987).
29. M. J. Turelli, J. H. Gillespie, T. W. Schoener, *Am. Nat.* **119**, 879 (1982).
30. J. F. Gilliam, R. F. Green, N. E. Pearson, *ibid.*, p. 875; H. P. Possingham, A. I. Houston, J. M. McNamara, *Ecology* **71**, 1622 (1990).
31. L. A. Real, S. Ellner, L. D. Harder, *Ecology* **71**, 1625 (1990).
32. R. Menzel, *Nature* **281**, 368 (1979); R. Menzel, in *Experimental Behavioral Ecology*, B. Holldobler and M. Lindauer, Eds. (Sinauer, Sunderland, MA, 1985), p. 55; B. Heinrich, in *The Biology of Learning*, P. Marler and H. Terrace, Eds. (Springer-Verlag, Heidelberg, 1984), p. 135.
33. R. Dukas and L. A. Real, unpublished manuscript.
34. N. M. Waser, *Am. Nat.* **127**, 593 (1986); R. Dukas and L. Real, unpublished manuscript.
35. W. F. Angermeier, *The Evolution of Operant Learning and Memory* (Karger, Basel, 1984); J. M. Pearce, *Introduction to Animal Cognition* (Erlbaum, London, 1987).
36. G. H. Pyke, in *The Ecology of Animal Movement*, I. R. Swingland and P. J. Greenwood, Eds. (Clarendon Press, Oxford, 1983), p. 7; D. E. Loria and F. R. Moore, *Behav. Ecol.* **1**, 24 (1990).
37. P. Feinsinger, *Ecol. Monogr.* **48**, 269 (1978); J. M. Pleasants and M. Zimmerman, *Oecologia* **41**, 283 (1979).
38. I. C. Cuthill *et al.*, *Anim. Behav.* **40**, 625 (1990).
39. G. A. Miller, *Psychol. Rev.* **63**, 81 (1956).
40. D. Kahneman and A. Tversky, *Econometrica* **47**, 263 (1979); U. Karmarkar, *Organ. Behav. Human Perform.* **21**, 61 (1979); M. Machina, *Econometrica* **50**, 277 (1982); R. C. Battalio, J. H. Kagel, D. N. MacDonald, *Am. Econ. Rev.* **75**, 597 (1985); J. H. Kagel, D. N. MacDonald, R. C. Battalio, *ibid.* **80**, 912 (1990); R. C. Battalio, J. H. Kagel, K. Jiranyakul, *J. Risk Uncertainty* **3**, 25 (1990).
41. M. Yaari, *Q. Journ. Econ.* **79**, 278 (1965); R. N. Rossett, *Rev. Econ. Stud.* **38**, 481 (1971); L. A. Real, *Am. Nat.* **130**, 399 (1987).
42. L. A. Real, R. Dukas, W. Zielinski, unpublished data.
43. L. A. Real, in *Behavioral Mechanisms in Diet Selection*, R. H. Hughes, Ed. (Springer-Verlag, Heidelberg, 1989), p. 1.
44. T. Getty, *Am. Nat.* **125**, 239 (1985); T. Getty and J. R. Krebs, *ibid.*, p. 39.
45. A. Tversky and D. Kahneman, *Science* **185**, 1124 (1974); D. Kahneman, P. Slovic, A. Tversky, Eds., *Judgement Under Uncertainty: Heuristics and Biases* (Cambridge Univ. Press, Cambridge, UK, 1982).
46. R. Dukas and L. A. Real, *Anim. Behav.*, in press.
47. I wish to thank L. Antony and J. Levine for their many helpful discussions on aspects of animal cognition; E. Werner, D. Real, S. Ellner, and three anonymous reviewers made many helpful suggestions on the manuscript. Supported by NSF grants BSR 8500203, BNS 8719292, and BNS 9096209.

Mid-Ocean Ridges: Discontinuities, Segments and Giant Cracks

KEN C. MACDONALD, DANIEL S. SCHEIRER, SUZANNE M. CARBOTTE

Geological observations reveal that mid-ocean ridges are segmented by numerous rigid and nonrigid discontinuities. A hierarchy of segmentation, ranging from large, long-lived segments to others that are small, migratory, and transient, determines the pattern and timing of creation of new ocean floor. To the extent that spreading segments behave like giant cracks in a plate, the crack propagation force at segment tips increases with segment length, which may explain why long segments tend to lengthen and prevail over shorter neighboring segments. Partial melting caused by decompression of the upper mantle due to plate separation and changes in the direction of spreading result in the spawning of new short segments so that a balance of long and short segments is maintained.

THE MID-OCEAN RIDGE IS THE LARGEST MOUNTAIN CHAIN and the most active system of volcanoes in the solar system. In plate tectonic theory, the ridge is located between plates of the earth's rigid outer shell that are separating at speeds of 10 to 170 mm/year. The ascent of molten rock from deep in the earth (~30 to 60 km) to fill the void between the plates creates new sea floor and a volcanically active ridge. This ridge system wraps around the globe like the seam of a baseball and is approximately 70,000 km long. However, the ridge itself is only ~5 to 30 km wide, very small compared to the plates, which can be thousands of kilometers across (Fig. 1).

The authors are with the Department of Geological Sciences and Marine Science Institute, University of California, Santa Barbara, CA 93106.

Early exploration showed that the gross morphology of spreading centers varies with the rate of plate separation. At slow spreading rates (10 to 40 mm/year) a rift valley 1 to 3 km deep marks the axis (*1*), while at fast spreading rates (90 to 170 mm/year) the axis is characterized by an elevation of the sea floor of several hundred meters (*2*). The rate of magma supply is a second factor that may influence the morphology of mid-ocean ridges. For example, a very high rate of magma supply can produce an axial high even where the spreading rate is slow; the Reykjanes Ridge south of Iceland is a good example. Also, for intermediate spreading rates (40 to 90 mm/year) the ridge crest may have either an axial high or rift valley, depending on the rate of magma supply (*3, 4*). Early mapping efforts also showed that the mid-ocean ridge is a discontinuous structure that is offset at right angles to its length at numerous transform faults.

During the past 7 years, an extraordinary confluence of diverse geologic observations of mid-ocean ridges has led to a series of advances in our understanding of sea floor spreading processes. Swath-mapping tools have been developed that can image large areas of the deep sea floor accurately. Structural maps based on these charts, combined with geochemical studies of rock samples, seismic and gravitational studies of velocity and density variations beneath the ridge, studies of sea floor magnetization, and near-bottom imaging of the distribution of hydrothermal vents, reveal a fundamental partitioning of the ridge into segments bounded by numerous discontinuities (*5–13*). These segments behave like giant cracks in the sea floor that can lengthen or shorten and have episodes of increased volcanic and tectonic activity. To the extent that individual segments behave as cracks in a brittle plate, it is possible to predict which segments will lengthen and prevail and which will shorten or even disappear. Although there remain areas of disagreement between some data sets and interpretations, the extent of agreement between such a large number of researchers using very different observations and tools is remarkable. In this article we summarize the implications for tectonic and volcanic processes at mid-ocean ridges, focusing on the broad concepts of segmentation and crack propagation.

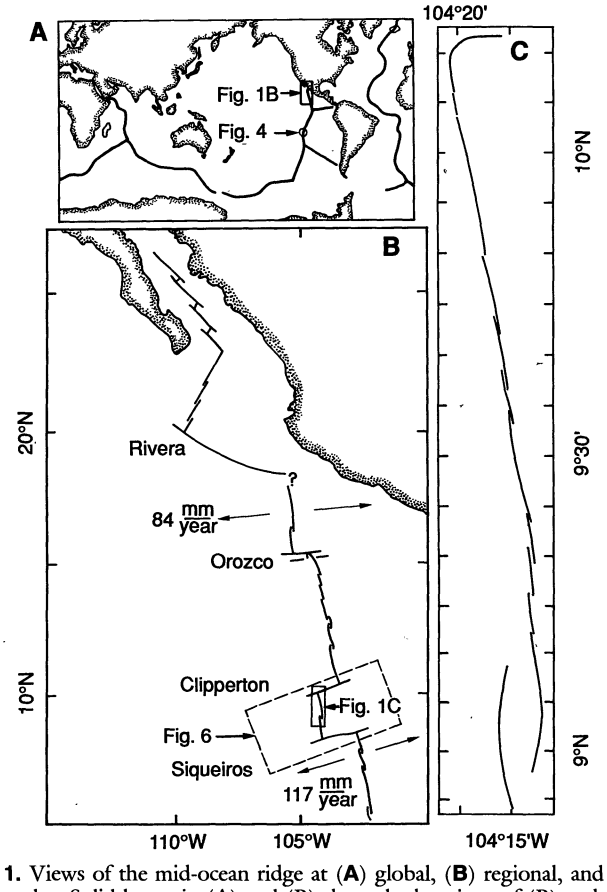

Fig. 1. Views of the mid-ocean ridge at (**A**) global, (**B**) regional, and (**C**) local scales. Solid boxes in (A) and (B) show the locations of (B) and (C), respectively, circle in (A) shows the location of the color image of Fig. 4, and dashed box in (B) shows the location of the color images of Fig. 6. (A) The mid-ocean ridge wraps around the globe like the stitching on a baseball. (B) A closer view of the mid-ocean ridge, in this case the northern EPR, shows that it is partitioned into segments [adapted from (*5, 6, 80*)]. (C) At a fine scale, the ridge is partitioned into higher order segments [adapted from (*48*)]. The example shown is the EPR, 9° to 10°N; the ridge offsets are all right-stepping (as expected for a continuing anticlockwise change in the direction of spreading) and less than 1 km (*13, 48*).

A Hierarchy of Segmentation

Most of the observations support the concept of a hierarchy in the segmentation of mid-ocean ridges (Table 1 and Fig. 2) [for reviews, see (*11, 14–16*)]. At higher orders, segments are shorter (less than 10 km for fourth order and up to 1000 km for first order) and more short-lived (from ~10^2 to 10^4 years for fourth order to ~10^7 years for first order) (Table 1 and Fig. 2). Discontinuities that define first-order segments are rigid plate transform faults (*17*), whereas finer scales of segmentation (orders 2 to 4) occur between transform faults (Fig. 2). Second-order ridge segments typically lengthen or shorten with time, last 0.5 to 10 million years, and terminate at discontinuities that are nonrigid. Overlapping spreading centers (OSCs) and oblique shear zones are examples of second-order discontinuities found at fast- and slow-spreading centers, respectively (*14, 18*). Segments of order three and four are very short-lived, on the order of 10^2 to 10^5 years (Table 1).

Segmentation can be seen clearly in the axial depth profiles of mid-ocean ridges (Fig. 3). Discontinuities of orders 1, 2, and 3 usually occur at local depth maxima, and the intervening midsections of segments are relatively shallow (Fig. 4). At slow-spreading ridges, marked by a rift valley, the floor of the valley shoals and narrows near midsegment. At fast-spreading ridges, characterized by an axial high, the ridge increases steadily in cross-sectional area toward the elevated midsections of individual segments (*19*).

Seismic measurements along the axis of the fast-spreading East Pacific Rise (EPR) reveal variations in the subaxial magma reservoir that correlate with the depth and shape of the rise (*10, 19*). This melt reservoir includes the axial magma chamber, which may be only a very thin lens of pure melt, and the larger encompassing reservoir of hot rock that contains a small amount of partial melt (*12, 20–23*) (Fig. 5, B and C). The reservoir is inflated to a cross-sectional area 5 to 6 km deep by 5 to 6 km wide beneath the shallow, swollen midsections of individual segments (*10, 20, 24*) (Fig. 5, B and C). The melt reservoir breaks at first-order discontinuities; it is reduced in cross-sectional area significantly and is commonly discontinuous at second-order discontinuities; it shrinks only slightly at third-order discontinuities and a few fourth-order discontinuities (*10, 20–22, 24–27*). Thus, a case can be made for a linkage between tectonic segmentation and the axial melt reservoir (*28*).

The relation between ridge segmentation and magma reservoir behavior is also reflected in geochemical variations of volcanic samples collected along the ridge axis (*11*). The data show that volcanic rocks at broad parts of segments have a higher percent by weight of MgO than those from the narrow parts of segments, generally near discontinuities. Although the data are noisy this difference suggests a tendency for hotter magmas to erupt near midsegment and cooler (farther from the source, perhaps) magmas to erupt near discontinuities (*11*). Virtually all segments of orders 1

to 3 have distinct geochemical signatures, as do at least 30% of the fourth-order segments (denser sampling may indicate that this percentage is even greater) (*11, 29*). Rocks sampled only slightly off-axis along the same fourth-order segments have different compositions from their on-axis counterparts (*30*). Thus, these fine scale segments must be very short-lived (*11*). The lack of any off-axis discordant zone further documents the brevity of third- and fourth-order segments (Table 1) relative to larger, longer-lived first- and second-order segments (*14*).

The off-axis discordant zones of second-order discontinuities reveal the history of segment evolution and magmatic activity. Many show a pattern of abandoned ridge tips and fossil OSC basins caused by repeated decapitation of ridge tips (Figs. 4, 6, 7, and 8) (*31, 32*). These propagation and decapitation events have a recurrence interval of 2×10^4 to 2×10^5 years. The average interval is $\sim 5 \times 10^4$ years (*7, 33, 34*). Three-dimensional (3-D) inversion solutions for crustal magnetization show that the discordant zones are highly magnetized (Fig. 6B), probably from the eruption of highly fractionated basalts near the discontinuities (*7, 34–37*). These basalts are diagnostic of a low and intermittent magma supply at discontinuities (*38*), consistent with structural and seismic evidence cited above.

A Magma Supply Model for Ridge Segmentation

The regular undulation of the crest of the ridge (which correlates with its cross-sectional area), the seismic evidence for an axial melt reservoir, the locations of discontinuities, and a host of other geologic observations (Table 1) have led to the development of a magma supply model for ridge segmentation in which the supply of melt from the upper mantle is enhanced beneath the shallow, swollen region of each segment and is depleted at the ends of each segment near OSCs and other discontinuities (*5, 10, 11, 14, 16, 19, 39*) (Fig. 5). As the plates spread apart, partial melting of mantle rocks occurs because of adiabatic decompression at depths of 30 to 60 km. The buoyant melt segregates from residual solid mantle and ascends to fill shallow magma chambers within the crust along the ridge axis. These melts locally swell the crustal magma reservoirs, and buoyant forces associated with the melt and surrounding halo of hot, melt-impregnated low-density rock create a local shoaling of the ridge crest.

Continuous injection of melt leads to local eruptions, migration of magma away from the locus of upwelling, and expansion of the axial magma chamber along strike. The laterally migrating magma loses hydraulic head with increasing distance from the center of magma replenishment; as a result, the depth of the ridge axis steadily increases along strike. As magma migrates at depth along the ridge, continued extension fractures the brittle carapace of frozen lava. Magmas then use these fractures as conduits to the sea floor, and volcanic eruptions follow the advancing crack front. The process outlined above occurs repeatedly as plate separation continues. In this magmatic model for a spreading center, ridge axis discontinuities occur at the distal ends of magmatic pulses and define the ends of ridge segments (Figs. 4 and 5).

Table 1. Characteristics of segmentation. References for segments are (*3–8, 14, 18, 33–36, 48–50, 53, 57, 62, 68, 75, 76, 79*). References for discontinuities are (*5–15, 17–27, 29–38, 40–44, 62–65*).

	Order 1	Order 2	Order 3	Order 4
		Segments		
Segment length (km)	600 ± 300* (400 ± 200)†	140 ± 90(50 ± 30)	50 ± 30 (15 ± 10?)	14 ± 8 (7 ± 5?)
Segment longevity (years)	>5 × 10^6	0.5 × 10^6 to 5 × 10^6 (0.5 × 10^6 to 10 × 10^6)	~10^4 to 10^5(?)	~10^2 to 10^4(?)
Rate of segment lengthening (long-term migration)	0 to 50 mm/year (0 to 30 mm/year?)	0 to 100 mm/year (0 to 30 mm/year)	Indeterminate—no off-axis trace	Indeterminate—no off-axis trace
Rate of segment lengthening (short-term propagation)	0 to 100 mm/year (?)	0 to 500 mm/year (0 to 50 mm/year)	Indeterminate—no off-axis trace	Indeterminate—no off-axis trace
		Discontinuities		
Type	Transform, large propagating rifts	Overlapping spreading centers (oblique shear zones, rift valley jogs)	Overlapping spreading centers (intervolcano gaps)	Devals, offsets of axial summit caldera (intravolcano gaps)
Offset (km)	>30 km	2 to 30 km	0.5 to 2.0 km	<1 km
Offset age (years)‡	>0.5 × 10^6 (>2 × 10^6)	<0.5 × 10^6 (<2 × 10^6)	~0	~0
Depth anomaly	300 to 600 m (500 to 2000 m)	100 to 300 m (300 to 1000 m)	30 to 100 m (50 to 300 m)	0 to 50 m (0 to 100 m?)
Off-axis trace	Fracture zone, pseudo-fault	V-shaped discordant zone	None	None
High amplitude magnetization?	Yes	Yes	Rarely (?)	No? (?)
Breaks in axial magma chamber?§	Always	Yes, except during OSC linkage? (N.A.)	Yes, except during OSC linkage? (N.A.)	Rarely, 4 of 21 for data through '90 (N.A.)
Break in axial low-velocity zone?	Yes (N.A.)	No, but reduction in volume (N.A.)	Small reduction in volume (N.A.)	Small reduction in volume? (N.A.)
Geochemical anomaly?	Yes	Yes	Usually	30 to 50%
Break in high-temperature venting?	Yes	Yes	Yes (N.A.)	Often (N.A.)

*± 1σ †Where information differs for slow- versus fast-spreading ridges (>60 mm/year), it is placed in parentheses. N.A. means nonapplicable (that is, a magma chamber has not been detected at slow-spreading centers yet, so a break in the chamber does not apply). A question mark means not presently known or poorly constrained. ‡Offset age refers to the age of the sea floor, which is juxtaposed to the spreading axis at a discontinuity. §The reflector of Detrick *et al.* (*10*) is assumed to be the roof of an axial magma chamber.

For slow-spreading ridges, seismic studies have not revealed a magma reservoir (*40*). However, a similar pattern of segmented upwelling may still occur there, and very small pockets of melt or highly episodic magma chambers may be present (Fig. 5C). Large "bull's-eye"–shaped gravity anomalies occur over ridge segments defined by second-order discontinuities on the Mid-Atlantic Ridge in some (*9, 41*) but not all cases (*42*). Corrected to remove the gravitational effects of topography, these anomalies indicate that low-density upper mantle or thickened oceanic crust is present beneath the midsections of segments. Kuo and Forsyth (*41*) proposed that these anomalies are best explained by a 3-D pattern of upwelling hot mantle material. The lack of such clearly defined gravity bull's-eyes over EPR segments has led some researchers to suggest that mantle upwelling may be more two dimensional there (*43*), although the distinctly 3-D distribution of an axial low-velocity zone beneath the EPR implies some degree of partitioning of melt beneath the ridge (*10, 22*).

Although the magma supply model fits the morphologic, structural, seismic, magnetic, and gravitational data, it only accounts for some aspects of the geochemical variability of rock samples from the ridge. The nongeochemical data tend to integrate over a long period of time, of the order of 10^3 to 10^5 years, whereas a basalt sample from part of a given flow unit represents an instantaneous sample of a small region of the magma reservoir. On short temporal and spatial scales, the history and pattern of melt delivery may be far more complicated than that envisaged in the magma supply model (*11*).

Ridge Segments as Giant Cracks: Why Long Segments Win

Several hypotheses have been offered to explain the causes of segmentation, segment lengthening, and propagation of discontinuities. One hypothesis is that the mid-ocean ridge is divided into stable spreading cells approximately 50 km long on the Mid-Atlantic Ridge and 80 km long on the EPR (*16, 44*). These cells are linked to uniformly spaced Rayleigh-Taylor–type gravitational instabilities in the upper mantle in which lower density diapirs of mantle melt ascend like hot air balloons through denser overlying mantle (*45, 46*). Melting continues as the mantle diapirs ascend and decompress (*45*). In this model ridge segmentation is driven by mantle buoyancy as opposed to passive, plate-controlled spreading. This model was modified to allow segment migration and rift propagation in which mantle melt anomalies are stable; that is, they are tied to a hot spot reference frame, and the off-axis wakes of discontinuities are hot spot tracks [see figure 2 of (*47*)]. Most discordant zones do not fit hot spot traces, however, and discontinuities along the same plate boundaries simultaneously migrate in different directions and at different rates (*14, 48, 49*).

Changes in spreading direction have been proposed as a mechanism for propagation and segment lengthening (*50*). Although there is no question that rift propagation provides a mechanism for ridge segments to orient perpendicular to a new spreading direction, a change in spreading direction does not provide adequate force to drive ridge propagation (*51*). Lonsdale (*49*) has proposed that segment lengthening and rift propagation tend to occur toward the pole of plate rotation during clockwise changes in spreading direction and away from the pole of opening during anticlockwise changes. This latter hypothesis offers no driving mechanism, and subsequent data sets demonstrate numerous counterexamples to this observation [for example, (*14, 48*)].

A more successful model involves gravitational spreading forces due to excess ridge axis topography (*51*). There is an undulation of axial depth on most ridges (Fig. 3), and the elevation of the axial region above its flanks represents gravitational potential energy. At a discontinuity, the segment with the greater gravitational spreading force (a function of its excess axial elevation) will lengthen and force the discontinuity to migrate "downhill" in the direction of lengthening (*52*). This model works well where hot spot magmatism has produced extraordinary ridge axis elevations and significant variations in near-field stress (*51, 53*) and is appealing because the gravitational spreading force at a given segment may fluctuate as magma supply to the segment waxes and wanes.

Crack Propagation Model for Segment Lengthening

We propose another mechanism for segment lengthening, which is additive to that of gravitational spreading: the crack propagation

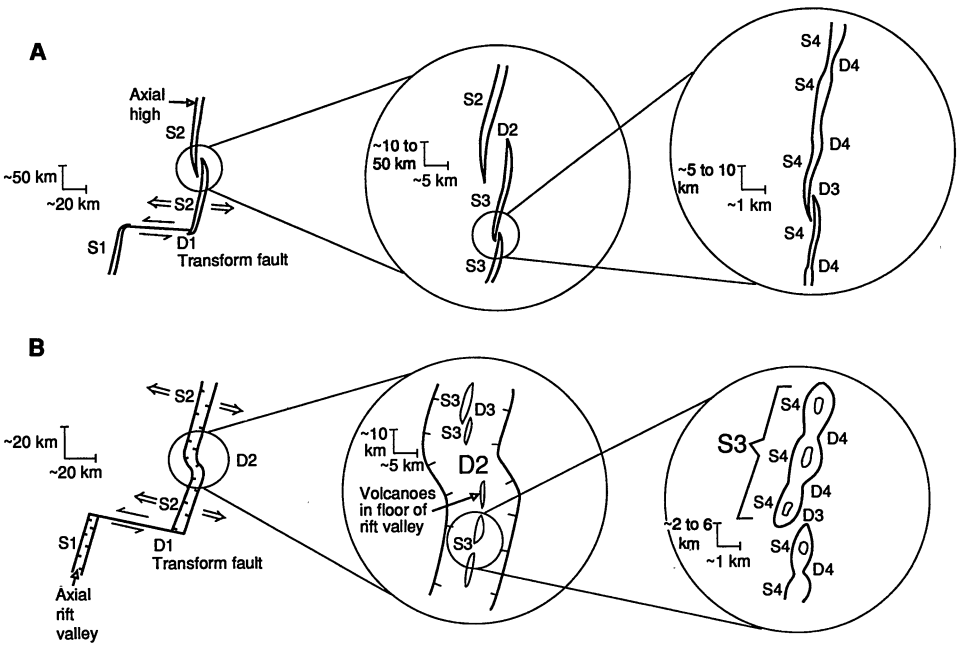

Fig. 2. A hierarchy of ridge segmentation defined by axial discontinuities for (**A**) fast- and (**B**) slow-spreading ridges. S1, S2, S3, and S4 are ridge segments of order 1, 2, 3, and 4 and D1, D2, D3, and D4 are ridge axis discontinuities of order 1, 2, 3, and 4. At both fast- and slow-spreading centers, first-order discontinuities are transform faults. Examples of second-order discontinuities are OSCs on fast-spreading ridges and oblique shear zones on slow-spreading ridges. Third-order discontinuities are small OSCs on fast-spreading ridges and intervolcano gaps on slow-spreading ridges. Fourth-order discontinuities are deviations from axial linearity (devals) resulting in slight bends or lateral offsets of the axis of less than 1 km on fast-spreading ridges and are intravolcano gaps on slow-spreading ridges. This four-tiered hierarchy of segmentation may really be a continuum. It has been established, for example, that fourth-order segments and discontinuities can grow to become third-, second-, and even first-order discontinuities and vice versa at both slow- and fast-spreading centers (*7, 18, 35, 44, 78*).

force, ΔG_F, caused by far-field plate stresses. This mechanism appeals to us because combined Sea Beam and SeaMARC II bathymetric data indicate that long spreading segments tend to lengthen at the expense of neighboring shorter segments (for example, near 9°N, Fig. 6). In fracture mechanics, the crack propagation force at the tip of a crack increases with crack length for an isolated crack. The far-field stress is tensile as the plates are pulled apart. Lachenbruch (*54*) estimated that this stress was 30 MPa, although more recent estimates range from 20 to 250 MPa (*55, 56*).

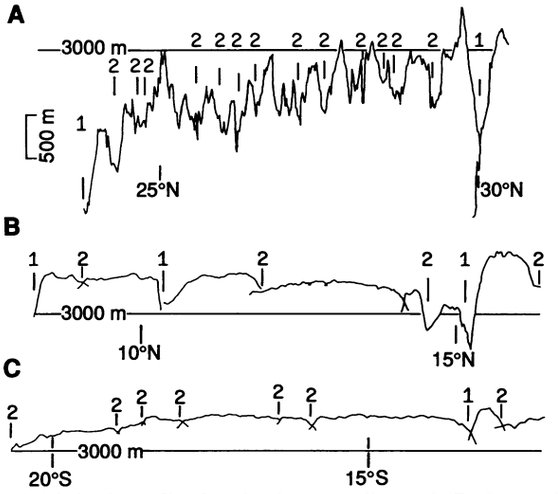

Fig. 3. Axial depth profiles for (**A**) slow-spreading and (**B**) fast- and (**C**) ultrafast-spreading ridges. Discontinuities of orders 1, 2, and 3 typically occur at local depth maxima (discontinuities of orders 3 and 4 not labeled here). The segments at fast-spreading rates are longer and have smoother axial depth profiles than those at slow-spreading rates. [(A) Adapted from (*8*); (B) adapted from (*81*); (C) adapted from (*33*)]. Vertical exaggeration = ×150.

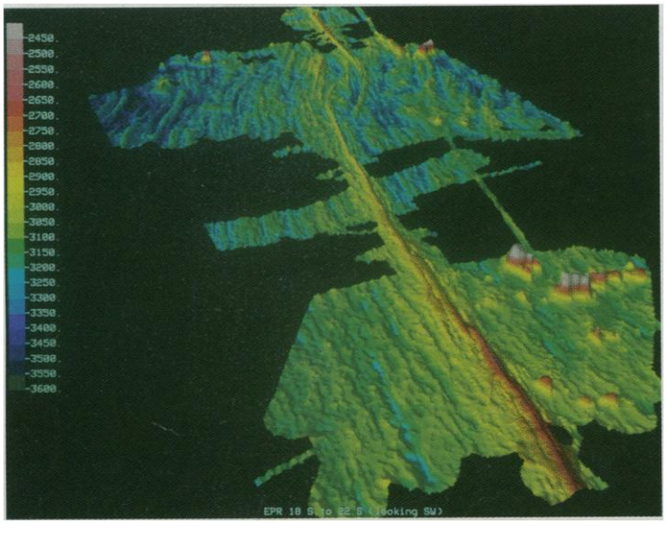

Fig. 4. Shaded relief image of the EPR 18° to 21°30′S looking southwest (produced by M.-H. Cormier; yellow color change is 2900 m, image is approximately 350 km long and 300 km across). An elevated, magmatically robust segment of the ridge occurs in the foreground. A large second-order discontinuity occurs in the background at 20°40′S (offset ~20 km). A series of abandoned ridge tips is evident on both flanks of the ridge near the discontinuity. They were clipped off during episodes of dueling propagation as the northern ridge segment lengthened southward and the southern segment lengthened northward (*33*). Averaged over 2 million years, the longer northern segment has won the duel, and a 20 mm/year net southward migration of the discontinuity has been produced. Seamount chains occur preferentially on the west flank of the ridge.

Because the plates do not accelerate away from the rise axis, far-field stresses must be balanced by resistive stresses associated with basal drag on the lithosphere, finite strength of the lithosphere at the rise axis, dynamic maintenance of axial rift valleys, and resistance to spreading at discontinuities. If far-field stresses were entirely balanced at the ridge axis, their role would be nullified. However, far-field stresses are not entirely balanced at the ridge axis, because (i) ridge propagation occurs even where there is no net excess topography along the axis [for example, in the South Atlantic (*35, 57*)] and (ii) spreading axes reorient themselves quickly to an orientation orthogonal to the direction of far-field least compressive stress (or spreading direction) (*48, 58*). Although this is an important unresolved issue, we assume that the net far-field stress acting at the ridge is 30 MPa (*54*).

We have focused above on second-order segments on the fast-spreading EPR. Third- and fourth-order segments and their discontinuities are too short-lived to leave off-axis traces, so segment lengthening cannot always be determined, and most first-order segments are restrained from significant lengthening and propagation by rigid-plate transform faults. To apply our crack model to spreading centers, we located all second-order discontinuities and defined their recent histories using continuous Sea Beam plus SeaMARC II bathymetric coverage along the EPR axis and its flanks between 18°N and 22°S. We used the same data to calculate the

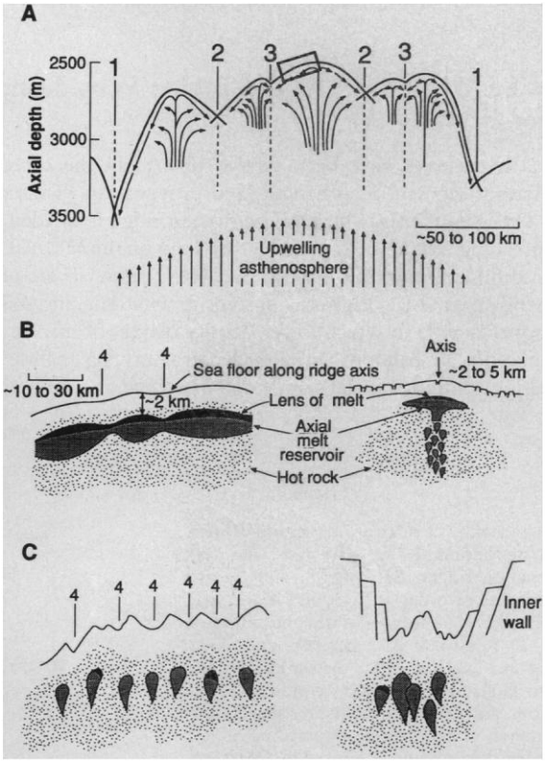

Fig. 5. Schematic diagram of how ridge segmentation may be related to mantle upwelling (**A**), and the distribution of magma supply (**B** and **C**) [adapted from (*14, 82, 83*)]. In (A), the depth scale applies only to the axial depth profile; numbers denote discontinuities and segments of orders 1 to 3. Decompression partial melting in upwelling asthenosphere occurs at depths 30 to 60 km beneath the ridge. As the melt ascends through a more slowly rising solid residuum, it is partitioned at different levels to feed segments of orders 1 to 3. The rectangle is an enlargement to show fine-scale segmentation for (B), a fast-spreading example, and (C), a slow-spreading example. In (B) and (C) along-strike cross sections showing hypothesized partitioning of the magma supply relative to fourth-order discontinuities (4's) and segments are shown on the left. Across-strike cross sections for fast- and slow-spreading ridges are shown on the right.

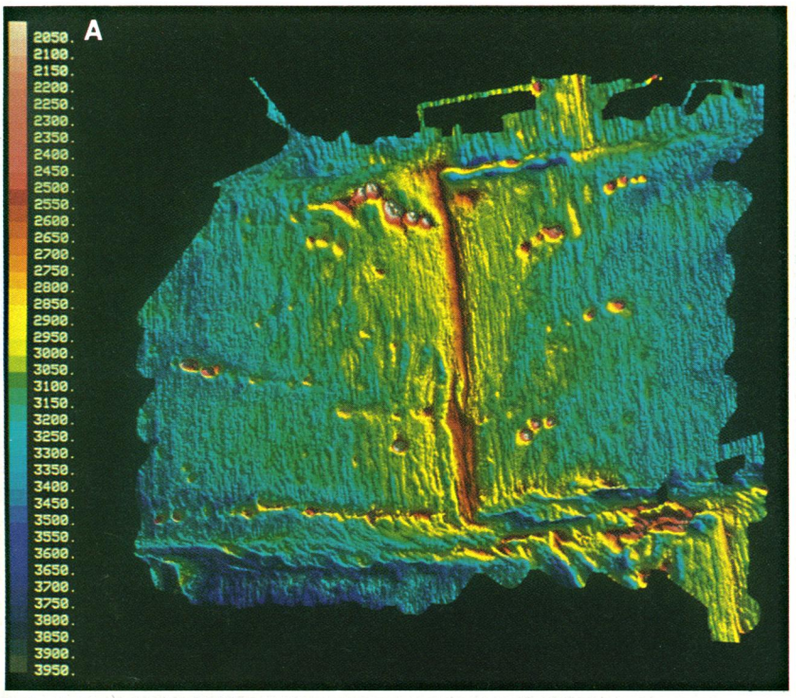

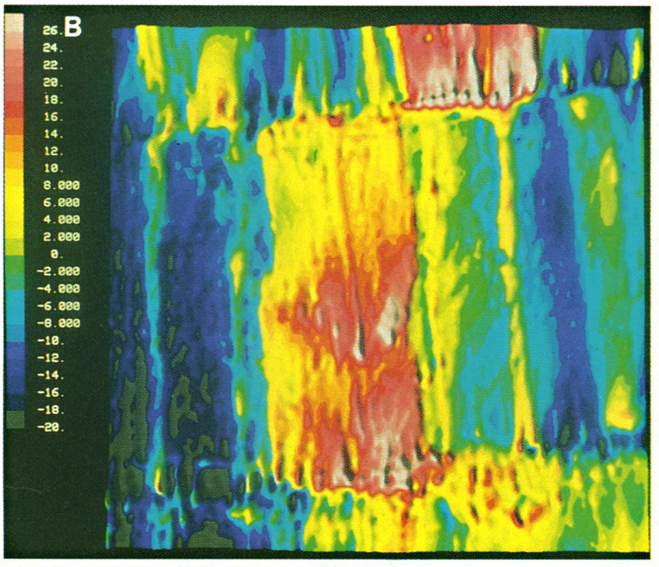

Fig. 6. Shaded relief images of the EPR showing (**A**) bathymetry and (**B**) 3-D magnetic inversion solution for crustal magnetization (viewed from above) (after *34*). The boundaries of the images are 10°40′N, 8°00′N, 102°45′W, and 105°30′W (105°50′W for the bathymetric image), and they are approximately 300 km by 300 km in size. On the ridge flanks adjacent to the 9°03′N OSC is a V-shaped discordant zone in the bathymetry and magnetization, indicating southward migration of the discontinuity at 52 mm/year within the past ~1.0 million years. The west flank discordant zone comprises abandoned curvilinear ridge tips that reflect episodic clipping of the western ridge tip at the OSC. The east flank discordant zone consists of greater depths with higher magnetizations. Southward migration of the discontinuity has not been steady but has involved a series of episodic and dueling propagation events with rates ranging from <10 mm/year to >500 mm/year. The longer northern segment is lengthening at the expense of the southern shorter segment, but its history over the last 1.8 Ma has been complex (see Fig. 7).

mode I (simple tension) stress intensity factors for the near-field gravitational spreading effects, K_{IN}, and the far-field plate stresses, K_{IF}. In calculating K_{IN}, we assumed that the near-field stresses driving crack propagation are the result of lithospheric pressure from anomalous ridge topography on the basis of an off-axis reference level 10 km from the ridge. Our analysis is based on the development of Phipps Morgan and Parmentier (*51*), although we use a formulation in which symmetric loading is not assumed (*59*). The crack propagation force, G, was calculated from K_I as described in Table 2. The critical factor in determining segment lengthening is ΔG, the difference in crack propagation force between two neighboring segments (*60*).

The results of our calculations and sea floor observations (Table 2 and Fig. 9) indicate the following: (i) the longer of the two segments at a discontinuity tends to lengthen at the expense of the shorter; (ii) K_{IF} and K_{IN} (which are additive) work in the same direction in most cases (except at the 16°20′N OSC); (iii) the far-field crack propagation force ΔG_F is at least two orders of magnitude larger than the near-field crack propagation force ΔG_N (ΔG_F is comparable to ΔG_N only if the far-field stresses are ~2 MPa); (iv) at the 16°20′N OSC, K_{IN} and ΔG_N predict that the southern, shorter segment will lengthen because of its extraordinary elevation relative to the rise flanks, but K_{IF} and ΔG_F correctly predict that the longer segment lengthens, as is observed; (v) on fast-spreading ridges, the longer segment with greater ΔG_F wins in 22 out of 24 cases—the only two counterexamples involve segments of nearly equal length in which both ΔG_F and ΔG_N fail to predict segment lengthening correctly; (vi) at slow-spreading ridges, the success rate is only 12 out of 18 (*61*).

Implications and Complications of the Crack Model

Far-field stresses and the increase of crack propagation force with segment length are not the only factors that control segmentation and migration of discontinuities. As mentioned above, the stress intensity factors associated with far-field stresses K_{IF} and gravitational spreading forces K_{IN} are additive, and the total crack propagation force can be considerably greater than that associated with far-field stresses alone (Table 2). The fact that dueling propagation is common, in which two segments alternately lengthen and dominate (*33, 62*), suggests that different forces control segment lengthening during the history of a given pair of ridge segments. For example, an episode of significant magma replenishment may elevate the axial depth profile of a shorter ridge segment so that near-field stresses dominate, and the migration of a nearby discontinuity might be reversed. Magma replenishment can also increase the magma pressure within dike intrusions beneath the ridge axis and further increase the role of near-field stresses.

In this simple treatment, we have ignored the interaction between pairs of cracks or segments (*63, 64*). Treatment of ridge segments as

isolated cracks may be a good first approximation because a brittle lid with finite strength and yield stress (10 to 20 MPa) may develop along the ridge axis during the lulls between major episodes of eruption and crack propagation. Thus, most of the crack propagation may occur outside of the region of two-crack interaction. Our observations indicate that fine-scale crack interaction, averaged over long periods of time (>100,000 years), will only act as a perturbation and produce short-lived reversals in the direction of long-term segment lengthening (*33*). Within this region of interaction, the tip of the segment that is becoming shorter must heal before the longer segment can continue lengthening (*31*). If it does not, dueling propagation may occur.

The crack model is less successful in predicting segment lengthening at slow-spreading centers than at fast-spreading centers, only predicting correctly the outcome in 12 out of 18 cases studied (Fig. 9). The rarity of the distinctive OSC geometry (as shown in Fig. 2A) also suggests that the slow-spreading centers are less well modeled by cracks in a brittle plate under tension than fast ones (*64*). The time-averaged thickness of zero-age oceanic lithosphere is greater on slow-spreading centers than that on fast ones (*22, 65*), perhaps thick enough to impede crack propagation. The mechanics of maintaining a deep axial rift valley may also complicate the stress field at slow-spreading centers (*54, 66*).

Outstanding Questions

If long segments grow at the expense of short segments, what prevents the ridge from becoming one very long segment? New small segments must be created at a rate that exceeds the ability for long segments to consume them. Given an average segment-lengthening rate of ~100 mm/year (*48*) and a typical fourth-order segment length of 10 km on fast-spreading ridges, new segments need to be created at least every 100,000 years. On slow-spreading centers where lengthening rates are slower, new segments need to be created at least every 0.5 million to 1 million years. If the magma supply model is a reasonable approximation of crustal accretion processes, then new fourth-order segments may be spawned more frequently than required by the segment-lengthening model presented here. Estimates of the frequency of major volcanic eruptions along the ridge vary from 10^2 to 10^5 years (*67, 68*).

Frequent perturbations to the local spreading direction may also spawn new segments. As more mid-ocean ridges are studied at a high resolution over large areas, it is becoming clear that most ridges experience frequent small changes in spreading direction. Some are caused by local changes in the direction of least compressive stress, and others represent movement of the pole of opening of two plates (*7, 34, 48, 50, 69*). A spreading plate boundary may rarely experience long periods of stable unidirectional spreading. Changes in the direction of spreading, whether local or regional, will spawn large numbers of third- and fourth-order segments that are oriented perpendicular to the new direction of least compressive stress (Figs. 1C and 7). Segments that are initially longer or engorged with melt will tend to lengthen and tap more melt anomalies, producing eruptions in the wake of the advancing crack front. Positive topographic relief, produced by the volcanism and upwelling, further contributes to crack propagation forces and lengthening of the segment. Smaller fourth- and third-order segments and discontinuities are swept up and incorporated in a smaller number of lengthening segments, with larger offsets at the bounding discontinuities (Fig. 7).

This cycle may rarely be completed, because new segments are spawned more rapidly than they are consumed. The EPR from 9° to 12°N is a good example (Fig. 1). A small clockwise change in spreading direction around 2.4 million years ago (Ma) followed by a nearly continuous anticlockwise change in the direction of spreading of 3° to 7° over the last 1.0 million years (*7, 34*) and continuing to the present has spawned numerous new fourth-order segments and discontinuities (Fig. 1C) (*48*). Some third-order segments and discontinuities have grown into larger second-order segments and discontinuities, for example, 9°N OSC (Fig. 7) and 11°45′N OSC (*7*). Thus, there is a dynamic equilibrium between the tendency for long segments to grow at the expense of short segments and the spawning of new short segments.

Is there linkage between tectonic, magmatic, and hydrothermal segmentation? We have stressed the agreement between diverse geologic data sets in defining segmentation, including structural, seismic, magnetic, gravitational, and geochemical observations (Table 1). New observations show that variations along the axis of the intensity of hydrothermal activity also correlate well with tectonic segmentation on the EPR from 9° to 10°N (Fig. 1) (*13*) and 12° to 13°N (*70, 71*). Hydrothermal activity and benthic faunal communities are abundant along fourth-order segments except at discontinuities, which are relative null points of activity. This distribution may be caused by emplacement of dikes as heat sources along the segments, which tend to terminate at discontinuities (*13, 22, 72*). Perhaps this pattern is not so surprising in the context of segments behaving as giant cracks. The same cracking phenomenon controls partial melting due to decompression, feeding of axial magma chambers, and dike emplacement. It also controls the growth of segments, development of discontinuities, and

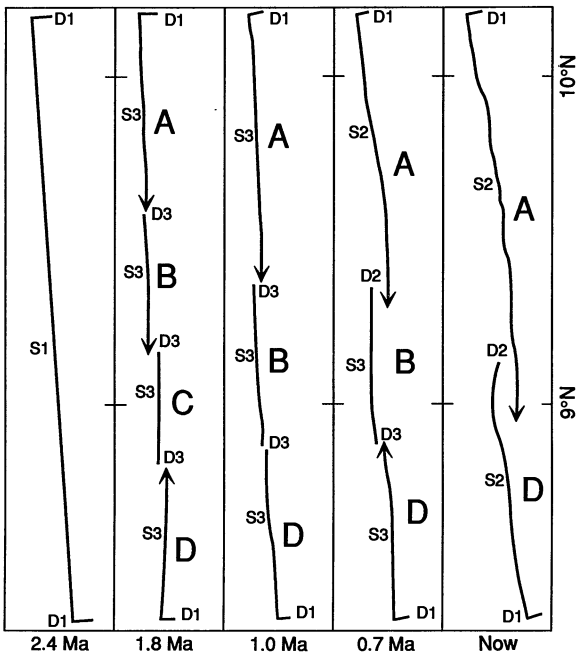

Fig. 7. Schematic history of segmentation between the Clipperton and Siqueiros transform faults since 2.4 Ma from bathymetric and magnetic data of Fig. 6. Arrowheads indicate the directions of segment growth. S1, S2, S3, D1, D2, and D3 refer to segments and discontinuities of orders 1, 2, and 3 as in Fig. 2. A first-order segment was partitioned into four third-order segments (A through D) during a small clockwise change in spreading direction. Segments C and B were then consumed as longer neighboring segments lengthened further. Four third-order segments eventually consolidated to two second-order segments. Also, since 1.8 Ma the spreading axis has rotated back anticlockwise approximately 6° and the sense of offset has changed at several discontinuities. In reconstructions of this nature, it is generally not possible to trace the histories of fourth-order segments, so they are not shown; however, continued anticlockwise rotation of the spreading axis has been accommodated by a recent spawning of fourth-order segments (Fig. 1C).

access of cold seawater to the interior of hot, recently intruded and erupted oceanic crust.

In many cases, however, magmatic and geochemical segmentation (derived from geochemistry of dredge rock samples) do not coincide very well with tectonic segmentation (derived from seismic, gravitational, magnetic, and bathymetric measurements). For example, the smallest of discontinuities may mark a major boundary between two segments with different geochemical characteristics (for example, 14°30′S and 11°08′N fourth-order discontinuities) (*11, 29*), whereas a major transform fault may be a relatively minor geochemical boundary (for example, Clipperton transform fault). Most (~60%) fourth-order tectonic discontinuities are not geochemical discontinuities (*48*); they may simply be the terminations of major individual fissure eruptions ~3 to 20 km in length along the plate boundary (*14*). If crack propagation forces do determine the lengths of spreading segments and the development of a segmentation pattern, this process may explain why the correspondence between geochemical and geophysical segmentation is imperfect. As a cracking front advances along the ridge axis, it is likely to intersect and tap a number of separate mantle melt sources [spaced ~5 km apart (*73*)]. Indeed, if segmentation is dominantly plate- and crack-controlled, then it is remarkable that geochemically defined segments coincide as frequently as they do with geophysically and tectonically defined segments.

If segment length and associated crack propagation forces determine the development of segmentation, does this suggest that the 3-D pattern of spreading is plate-controlled and thus primarily passive? We suggest that there is a feedback between passive and active mechanisms. Magma supply beneath the ridge axis will tend to be enhanced over loci of partial melting in the upper mantle (Fig. 5), and in the presence of magma, crustal failure can occur at much lower deviatoric stresses (*74*). When a new episode of extension occurs along the mid-ocean ridge, the thin, healed lithosphere along the axis will break where the magma pressure and supply is greatest, and cracking fronts will advance in both directions away from these magmatically robust regions. Such regions may occur beneath initially short segments (*75, 76*) or even within transform faults [for example, the robust mid-Yaquina spreading center (*49*) and the spreading centers within the Siqueiros transform fault (*73*)]. At slow-spreading ridges, the flux of magma may not be adequate to supply a lengthening crack, and volcanism may remain localized at a point source except during rare episodes of abundant magma supply

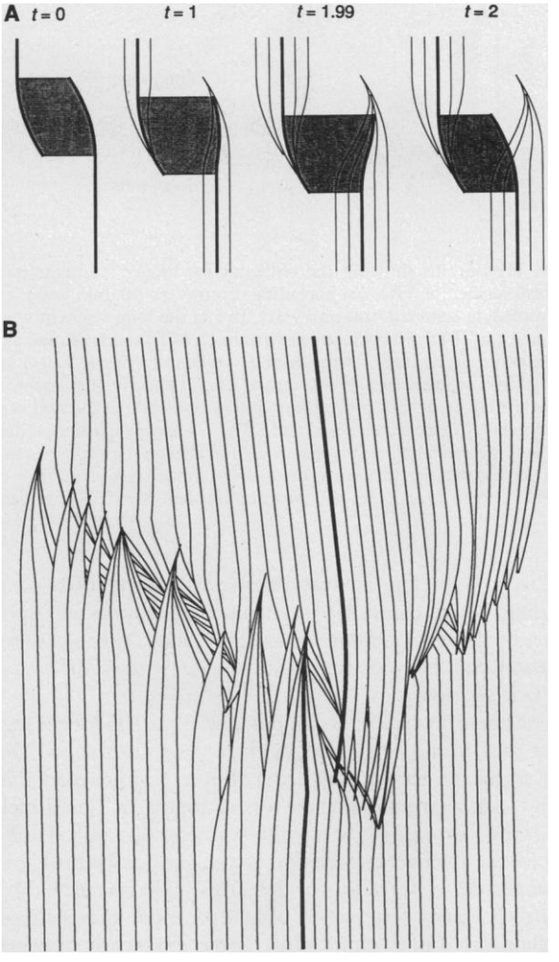

Fig. 8. (**A**) Step-by-step kinematic evolution of an OSC showing decapitation of the advancing ridge tip as the new ridge tip cuts inside of the old one (after *32*). Time is denoted by t in arbitrary units. Heavy line is the spreading axis. (**B**) Kinematic history of the EPR near 9°N, applying the model in (A) (from *34*). This example shows how lengthening and shortening of neighboring ridge segments and the clipping-off of ridge tips near discontinuities (second-order in this case) are important to mid-ocean ridge evolution and produce complex off-axis discordant zones on the sea floor.

Table 2. Crack propagation forces for selected ridge segments. Results of 4 of our 24 calculations for near-field and far-field crack propagation forces for fast-spreading centers. K_{IN} is the near-field mode I stress intensity factor; K_{IF} is the far-field mode I stress intensity factor. $K_{IF} = \sigma_{11F}(\pi L)^{1/2}$, σ_{11F} is the far-field stress, L is the half length of the segment.

$$K_{IN} = (\pi L)^{-1/2} \int_{-L}^{L} \sigma_{11N}(y) dy \left(\frac{L + y}{L - y} \right)^{1/2}$$

$\sigma_{11N}(y)$ is the normal stress acting along the crack or segment wall (*59*). $G_F = K_{IF}^2/E$; E is Young's modulus, assumed to be 10^{11} Pa (*79*). $G_N = K_{IN}^2/E$. $G_T = (K_{IF} + K_{IN})^2/E$ (total crack propagation force, near-field plus far-field). Long segments have a greater crack or segment propagation force than do short segments. For an assumed far-field stress of 30 MPa (used here), the role of far-field stress is more important than that of near-field stress. If the net far-field stress is ~2 MPa, then the roles of near- and far-field stresses are comparable.

Discontinuity	Neighboring segments	Segment lengths (km)	K_{IF} (Pa · m$^{1/2}$ × 10^9)	K_{IN}	ΔG_F (N × 10^7)	ΔG_N (N × 10^7)	ΔG_T (N × 10^7)
16°20′N OSC	18°00′N to 16°20′N	205	17	0.8	128	−0.17	80
	16°20′N to 15°25′N	112	12.7	0.9			
11°45′N OSC	14°30′N to 11°40′N	325	21.5	1.5	212	1.0	243
	11°50′N to 10°20′N	177	15.8	1.1			
9°N OSC	10°10′N to 8°55′N	138	14.4	0.8	90	0.39	103
	9°10′N to 8°20′N	85	10.8	0.5			
20°40′S OSC	18°35′S to 20°40′S	225	17.9	1.4	148	1.9	193
	20°40′S to 21°45′S	120	13.1	0.3			

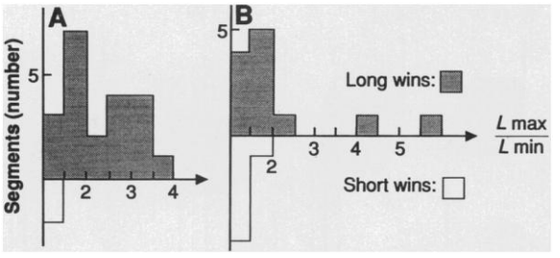

Fig. 9. Histograms showing the tendency for longer segments to win or lengthen farther at (**A**) fast-spreading centers (>60 mm/year) and (**B**) slow-spreading centers (<60 mm/year). In (A) the long segment wins in 22 of 24 cases; in (B) the long segment wins in 12 of 18 cases. Plotted along the horizontal axis is the ratio of the present-day lengths of the longer segment to the shorter segment at a discontinuity. This is directly proportional to the ratio of the far-field crack propagation forces operating at the two neighboring segment tips (see Table 2 and text). The crack propagation model works better for fast-spreading ridges than for slow; also, in the counterexamples in which the shorter segment wins, the ratio of the segment lengths is close to one. [Data from (*5, 33, 48, 49*) and unpublished SeaMARC II data 3° to 23°S]

(Fig. 5C) (77). The feedback between passive, plate-controlled spreading (crack-controlled segmentation) and active spreading (driven by upwelling and magma supply) may explain why tectonic segmentation does occasionally correlate with geochemical and magmatic segmentation.

There are many other outstanding questions. Do longer segments extract melt from deeper regions than shorter segments? Do first-order segments extract melt from deeper regions than third- or fourth-order segments? Is there a partitioning of partial melt as it ascends that corresponds to tectonic segments (as implied in Fig. 5)? What is the relative importance of the various controls of ridge segmentation? Is spreading and accretion of oceanic lithosphere primarily a passive response to plate separation, or is active mantle upwelling more important? What is the interaction between segment lengthening through crack propagation and mantle upwelling beneath the ridge? On a very different tack, is the distribution and development of mid-ocean ridge faunal communities controlled by ridge segmentation? Further progress on both observational and theoretical fronts, such as that coordinated by the RIDGE (Ridge Interdisciplinary Global Experiments) program, is needed to help answer these questions.

REFERENCES AND NOTES

1. B. C. Heezen, *Sci. Am.* **203**, 99 (October 1960).
2. H. W. Menard, *Science* **132**, 1737 (1960).
3. K. C. Macdonald, in *The Geology of North America*, vol. M of *The Western North Atlantic Region*, P. R. Vogt and B. E. Tucholke, Eds. (Geological Society of America, Boulder, CO, 1986), pp. 51–68.
4. J.-C. Sempere *et al.*, *Geology* **19**, 429 (1991).
5. K. C. Macdonald, J.-C. Sempere, P. J. Fox, *J. Geophys. Res.* **89**, 6049 (1984).
6. P. Lonsdale, *Geol. Soc. Am. Bull.* **96**, 313 (1985).
7. L. J. Perram and K. C. Macdonald, *J. Geophys. Res.* **95**, 21363 (1990).
8. J.-C. Sempere, G. M. Purdy, H. Schouten, *Nature* **344**, 427 (1990).
9. J. Lin, G. M. Purdy, H. Schouten, J.-C. Sempere, C. Zervas, *ibid.*, p. 627.
10. R. S. Detrick *et al.*, *ibid.* **326**, 35 (1987).
11. C. M. Langmuir, J. F. Bender, R. Batiza, *ibid.* **322**, 422 (1986).
12. J. A. Madsen, R. S. Detrick, J. C. Mutter, P. Buhl, J. A. Orcutt, *J. Geophys. Res.* **95**, 4967 (1990).
13. R. M. Haymon *et al.*, *Earth Planet. Sci. Lett.* **104**, 513 (1991).
14. K. C. Macdonald *et al.*, *Nature* **335**, 217 (1988).
15. K. C. Macdonald and P. J. Fox, *Sci. Am.* **262** (no. 6), 72 (1990).
16. H. Schouten, K. D. Klitgord, J. A. Whitehead, *Nature* **317**, 225 (1985).
17. P. J. Fox and D. G. Gallo, *Tectonophysics* **104**, 205 (1984).
18. N. R. Grindlay, P. J. Fox, K. C. Macdonald, *Mar. Geophys. Res.* **13**, 21 (1991).
19. K. C. Macdonald and P. J. Fox, *Earth Planet. Sci. Lett.* **88**, 119 (1988).
20. E. E. Vera *et al.*, *J. Geophys. Res.* **95**, 15529 (1990).
21. G. M. Kent, A. J. Harding, J. A. Orcutt, *Nature* **344**, 650 (1990).
22. D. R. Toomey *et al.*, *ibid.* **347**, 639 (1990).
23. D. W. Caress, M. S. Burnett, J. A. Orcutt, *J. Geophys. Res.*, in press.
24. M. S. Burnett, D. W. Caress, J. A. Orcutt, *Nature* **339**, 206 (1989).
25. J. C. Mutter *et al.*, *ibid.* **336**, 156 (1988).
26. A. J. Harding *et al.*, *J. Geophys. Res.* **94**, 12163 (1989).
27. A. Harding, G. Kent, M. Kappus, J. Orcutt, *RIDGE Events* **2**, 8 (1991).
28. There are exceptions to this orderly pattern of magma distribution; the magma chamber may wander 1 to 2 km away from the axis (*25*), and magma may occasionally pool or accumulate near a discontinuity (*27*).
29. J. M. Sinton, S. M. Smaglik, J. J. Mahoney, K. C. Macdonald, *J. Geophys. Res.* **96**, 6133 (1991).
30. J. R. Reynolds, C. H. Langmuir, E. Humler, J. F. Bender, *Eos* **71**, 1629 (1990).
31. K. C. Macdonald, J.-C. Sempere, P. J. Fox, R. C. Tyce, *Geology* **15**, 993 (1987).
32. D. S. Wilson, *Earth Planet. Sci. Lett.* **96**, 384 (1990).
33. K. C. Macdonald, R. M. Haymon, S. P. Miller, J.-C. Sempere, P. J. Fox, *J. Geophys. Res.* **93**, 2875 (1988).
34. S. M. Carbotte and K. C. Macdonald, *ibid.*, in press.
35. S. M. Carbotte, S. M. Welch, K. C. Macdonald, *Mar. Geophys. Res.* **13**, 51 (1991).
36. J.-C. Sempere *et al.*, *Geophys. J. R. Astron. Soc.* **79**, 799 (1984).
37. J.-C. Sempere, *Earth Planet. Sci. Lett.*, in press.
38. D. M. Christie and J. M. Sinton, *ibid.* **56**, 321 (1981).
39. M. P. Ryan, *U.S. Geol. Surv. Prof. Pap. 1350* (1987), p. 1395.
40. R. S. Detrick, J. C. Mutter, P. Buhl, I. I. Kim, *Nature* **347**, 61 (1990).
41. B.-Y. Kuo and D. W. Forsyth, *Mar. Geophys. Res.* **10**, 205 (1988).
42. D. K. Blackman and D. W. Forsyth, *J. Geophys. Res.* **96**, 11741 (1991).
43. J. Lin and J. Phipps Morgan, *Geophys. Res. Lett.*, in press.
44. H. Schouten and K. D. Klitgord, *Earth Planet. Sci. Lett.* **59**, 255 (1982).
45. J. A. Whitehead, H. J. B. Dick, H. Schouten, *Nature* **312**, 146 (1984).
46. K. Crane, *Earth Planet. Sci. Lett.* **72**, 405 (1985).
47. H. Schouten, H. J. B. Dick, K. D. Klitgord, *Nature* **326**, 835 (1987).
48. K. C. Macdonald *et al.*, *Mar. Geophys. Res.*, in press.
49. P. Lonsdale, *J. Geophys. Res.* **94**, 12197 (1989).
50. R. N. Hey, F. K. Duennebier, W. J. Morgan, *ibid.* **85**, 3647 (1980).
51. J. Phipps Morgan and E. M. Parmentier, *ibid.* **90**, 8603 (1985).
52. This is an oversimplification of their model because they consider a balance of forces at the crack tip and treat the crack as being isolated.
53. R. N. Hey, M. C. Kleinrock, S. P. Miller, T. M. Atwater, R. C. Searle, *J. Geophys. Res.* **91**, 3369 (1986).
54. A. H. Lachenbruch, *ibid.* **78**, 3395 (1973).
55. F. A. Dahlen, *ibid.* **86**, 7801 (1981).
56. S. R. Bratt, E. A. Bergman, S. C. Solomon, *ibid.* **90**, 10249 (1985).
57. J. M. Brozena and R. S. White, *Nature* **348**, 149 (1990).
58. K. C. Macdonald, *Geol. Soc. Am. Bull.* **88**, 541 (1977).
59. D. J. Cartwright and D. P. Rooke, in *Fracture Mechanics: Current Status, Future Prospects*, R. A. Smith, Ed. (Pergamon, New York, 1979), pp. 91–124.
60. We have not attempted a complete analysis of the balance of forces governing crack propagation. Our purpose is to call attention to the possible importance of far-field stresses in controlling segmentation and its evolution.
61. We have also observed a preferential lengthening of initially longer segments using wax models of separating plates in experiments similar to those conducted by D. W. Oldenburg and J. N. Brune [*J. Geophys. Res.* **80**, 2575 (1975)].
62. H. P. Johnson *et al.*, *ibid.* **88**, 2297 (1983).
63. D. D. Pollard and A. Aydin, *ibid.* **89**, 10017 (1984).
64. J.-C. Sempere and K. C. Macdonald, *Tectonics* **5**, 151 (1986).
65. D. R. Toomey, S. C. Solomon, G. M. Purdy, *J. Geophys. Res.* **93**, 9093 (1988).
66. J. Lin and E. M. Parmentier, *Geophys. J.* **96**, 1 (1989).
67. K. C. Macdonald, *Annu. Rev. Earth Planet. Sci.* **10**, 155 (1982).
68. R. A. Pockalney, R. S. Detrick, P. J. Fox, *J. Geophys. Res.* **93**, 3179 (1988).
69. F. Pollitz, *Nature* **320**, 738 (1986).
70. P. Gente, J. M. Auzende, V. Renard, Y. Fouquet, D. Bideau, *Earth Planet. Sci. Lett.* **78**, 224 (1986).
71. C. Lalou, E. Brichet, R. Hekinian, *ibid.* **75**, 59 (1985).
72. G. M. Purdy *et al.*, *Eos* **72**, 262 (abstr.) (1991).
73. D. J. Fornari *et al.*, *Mar. Geophys. Res.* **11**, 263 (1989).
74. A. M. Rubin and D. D. Pollard, *Geology* **16**, 413 (1988).
75. D. W. Forsyth, D. K. Blackman, G. A. Neumann, *Eos* **71**, 1628 (abstr.) (1990).
76. P. Patriat *et al.*, *ibid.*, p. 1629 (abstr.).
77. D. K. Smith and J. R. Cann, *Nature* **348**, 152 (1990).
78. P. J. Fox, N. R. Grindlay, K. C. Macdonald, *Mar. Geophys. Res.* **13**, 1 (1991).
79. D. L. Turcotte and G. Schubert, *Geodynamics Applications of Continuum Physics to Geological Problems* (Wiley, New York, 1984).
80. T. M. Atwater and J. Severinghaus, in *The Geology of North America*, vol. N of *The Eastern Pacific Ocean and Hawaii*, E. L. Winterer, D. M. Hussong, R. W. Decker, Eds. (Geological Society of America, Boulder, CO, 1989), pp. 15–20.
81. K. C. Macdonald, *ibid.*, pp. 93–110.
82. ———, *Nature* **348**, 108 (1990).
83. C. H. Langmuir, *ibid.* **326**, 15 (1987).

84. We thank the Office of Naval Research (N00014-90-J1G45) and the NSF (OCE89-11587) for supporting this research. A. Rubin, J.-C. Sempere, P. J. Fox, J. Phipps Morgan, R. Haymon, D. Pollard, D. Wilson, and R. N. Hey helped with stimulating discussions and careful reviews of the manuscript, M.-H. Cormier helped with reduction of data and Fig. 4, and A. Macias and A. Padgett prepared the illustrations. We also thank the scientific parties, officers, and crew of the MW8706, MW8707, MW8710, and RAPA I expeditions for their cooperation in helping collect the data shown in Figs. 4 and 6.